Sol-gel synthesis of Ni/Al_2O_3 catalysts for toluene reforming: Support modification with alkali, alkaline earth or rare-earth dopant (Ca, K, Mg or Ce)

Vincent Claude , Julien G. Mahy , Timothée Lohay ,
Rémi G. Tilkin , Francesca Micheli , Stéphanie D. Lambert

PII: S2468-0230(20)30141-3
DOI: https://doi.org/10.1016/j.surfin.2020.100511
Reference: SURFIN 100511

To appear in: *Surfaces and Interfaces*

Received date: 26 February 2020
Revised date: 16 March 2020
Accepted date: 17 March 2020

Please cite this article as: Vincent Claude , Julien G. Mahy , Timothée Lohay , Rémi G. Tilkin , Francesca Micheli , Stéphanie D. Lambert , Sol-gel synthesis of Ni/Al_2O_3 catalysts for toluene reforming: Support modification with alkali, alkaline earth or rare-earth dopant (Ca, K, Mg or Ce), *Surfaces and Interfaces* (2020), doi: https://doi.org/10.1016/j.surfin.2020.100511

Highlights

- Sol-gel Ni/γ-Al_2O_3 catalysts were modified with alkali, alkaline earth or rare-earth.
- The sol-gel synthesis is carried out in water medium in soft conditions.
- Single doping of support reduces the carbon deposition up to 40%.
- The combination of K and Ca leads to a high toluene conversion (60 %).

Sol-gel synthesis of Ni/Al_2O_3 catalysts for toluene reforming: Support modification with alkali, alkaline earth or rare-earth dopant (Ca, K, Mg or Ce)

Vincent Claude[1], Julien G. Mahy[1, 2*], Timothée Lohay[1], Rémi G. Tilkin [1, 3], Francesca Micheli[4], Stéphanie D. Lambert[1]

[1] *Department of Chemical Engineering – Nanomaterials, Catalysis & Electrochemistry, University of Liège, B6a, Quartier Agora, Allée du six Août 11, 4000 Liège, Belgium*

[2] *Institute of Condensed Matter and Nanosciences (IMCN), Université catholique de Louvain, Place Louis Pasteur 1, 1348, Louvain-la-Neuve, Belgium*

[3] *Centre Interfacultaire des Biomatériaux (CEIB), University of Liège, Allée du Six Août 11, 4000 Liège, Belgium*

[4] *Department of Industrial Engineering, University of L'Aquila, 18 via G. Gronchi, 67100 L'Aquila, Italy*

***Corresponding author:** Julien G. Mahy, Institute of Condensed Matter and Nanosciences (IMCN), Université catholique de Louvain, Place Louis Pasteur 1, 1348, Louvain-la-Neuve, Belgium. E-mail address: julien.mahy@uclouvain.be.

Keywords: Ni/Al_2O_3; Sol-Gel process; Toluene reforming; Oxide modification

Abstract

In this study, the influence of alkali, alkaline earth or rare-earth dopant (*i.e.* Ca, K, Mg or Ce) addition in 10 wt. % $Ni/\gamma\text{-}Al_2O_3$ catalyst were studied on the material physicochemical properties and catalytic activity. Twelve doped $Ni/\gamma\text{-}Al_2O_3$ catalysts were synthesized by sol-gel process in aqueous medium. One $Ni/\gamma\text{-}Al_2O_3$ catalyst without dopant was also synthesized as reference material. The addition of 1.5 wt. % of alkali (*i.e.* Ca, K or Mg) did not influence the acido-basicity properties of the catalysts due to low interactions with the support. All samples doped with 1.5 wt. % of oxide (*i.e.* Ca, K, Mg or Ce) presented a decrease of benzene

selectivity up to 73% and a decrease of the amount of carbon deposit up to 40 %. These results were attributed to a higher degradation of the intermediate compounds of toluene and the carbonaceous compounds because of a higher amount of H_2O and CO_2 molecules adsorbed on these oxides. Among the different compositions of Ni/γ-Al_2O_3 catalysts doped with two different types of oxides (*i.e.* K+Ca) showed the most interesting performances with an increase of 20 % in conversion and a decrease of 10 % in carbon deposition. Therefore, it showed that low-cost elements (as Ca and K) can be added in small amount to increase the catalytic properties without the need of the expensive ceria element.

1. Introduction

Adapted from old coal gasification technologies developed during the industrial revolution, the biomass gasification appears nowadays as an interesting and versatile way to take advantage of different sources (*e.g.* agricultural and urban wastes, energy crops, food and industrial processing residues). If managed conscientiously, these processes can therefore lead to the sustainable and renewable production of a bio-syngas, which can either be directly used as combustible or converted into storable and high valuable chemical compounds [1,2].

However, the reactors can have some technical problems, limiting their development [1–4]. The problems are mainly due to the formation of tars that can soot the reactor and the pipes.

In the recent decade, nanomaterials have attracted increasing attention for the development of functional materials in a large range of applications in catalytic reactions with a large range of synthesis methods. For examples, different metal oxides can be obtained by thermal decomposition [5–8] and used in electrochemical or photocatalytic applications. Zeolites modified with metallic ions can be obtained and used for oxidation reactions [9–12]. Different semi-conductors catalysts can be synthesized with specific morphologies [13–15].

For the removing of tars, many works have shown the possibility to use nanocatalysts eliminating tars via reforming reactions [1,3,16–21].

Depending the catalyst location, different material properties will be required: within the reactor for primary catalyst or outside the reactor with secondary catalyst. This work focused on secondary catalytic materials working around 650 °C without mechanical stress.

For tar removal, Ni-based catalysts are often referred as the most efficient materials with a loading in the range of 15-20 wt. % [1]. The Ni active phase is commonly deposited on various substrates as Alumina, Zirconia, Zeolites or Olivine. γ-Al_2O_3 phase is especially pointed as the best support for secondary catalyst applications [16,21–24] and many works have tried to optimize its properties, as acidity/basicity or resistance to sintering, thanks to doping.

In this work, oxide dopants (CaO, MgO, K_2O, and CeO_2) have been investigated to increase the activity and lifetime of Ni/Al_2O_3 catalysts. Indeed, these dopants present positive interactions with the alumina support of the catalysts.

Adding CaO to γ-Al_2O_3 allows keeping a high dispersion of particles [25]. Furthermore, when the calcination temperature is sufficiently high (T ~ 900 °C) [26], mayenite structure ($Ca_{12}Al_{14}O_{33}$) can be formed. Mayenite shows a very good anti-coking and anti-sulfur properties thanks to the presence of “free oxygen” in its structure [27].

In addition to the interesting properties of magnesium (*i.e.* Ni-MgO interactions, CO_2 adsorption), under the adequate calcination temperature (T ~ 800°C) [28,29], the formation of magnesium aluminate spinel ($MgAl_2O_4$) considerably increases the mechanical strength and the sintering resistance of the catalyst [30].

Among a series of different additives (*i.e.* Na, K, Mg, Ca, Ba, La, Zr or Ce) deposited on γ-Al_2O_3 support, Seok *et al.* [31] showed that K was the most efficient against coking. This effect was researched thoroughly by Gálvez *et al.* [32], who suggested that after calcination at

$T > 650°C$, the formation of K_2O was possible. Under a syngas atmosphere, K_2O is immediately transformed into K_2CO_3 or KOH, which favor the formation of reactive O^* and HO^* species.

Despite its high price, cerium oxide appears to be the most promising support doping element discovered in the last two decades. Indeed, cerium oxide can easily stock and destock oxygen, which increases its redox properties and its oxygen lability, thus strongly inhibiting the surface carbon formation. Wang *et al.* [33] investigated the dry reforming of methane with Ni catalysts supported on γ-Al_2O_3, CeO_2, and CeO_2/γ-Al_2O_3. The catalytic performances were the best for the composition Ni/CeO_2/γ-Al_2O_3, followed by Ni/γ-Al_2O_3, and finally Ni/CeO_2. The authors highlighted the fact that adding CeO_2 to γ-Al_2O_3 generates strong metal-support interactions, resulting in a higher dispersion of Ni nanoparticles and an increased resistance against sintering.

However, the diverse methods used for the preparation of the catalysts and the numerous conditions of catalytic tests existing in the literature made the comparison of the influences of these elements very difficult. Therefore, the main objective of this work is to perform a large screening in order to highlight some interesting combinations of elements. In this work, the synthesis method is the same for all the catalysts and consists in the use of the sol-gel process. This method is known to highly disperse dopants or active sites in another matrix in only one step [34–37] and allows soft synthesis conditions [38,39].

In this work, 10 wt. % Ni/γ-Al_2O_3 catalysts were modified with 1.5 wt. % of alkali, alkaline earth or rare earth (*i.e.* Mg, Ca, K or Ce) in order to increase their catalytic activity on the toluene reforming and increase their resistance to coking. Double doping (1.5 wt. % for each dopant) was also investigated in order to highlight potential synergistic influences. From the catalytic results of the single-doped samples, Ni/γ-Al_2O_3 catalysts were also modified with 3 wt. % of the most promising oxides (*i.e.* Ca and K). The influence of the dopants on the physico-chemical and catalytic properties were studied thanks to a large range of

characterizations and catalytic experiments at 650 °C for the reforming of 24,000 ppmv of toluene.

2. Materials and Methods

2.1. Catalyst synthesis

Aluminum nitrate nonahydrate ($Al(NO_3)_3.9H_2O$, ACS reagent, ≥ 98 %, Sigma-Aldrich), NH_4OH solution (28 % NH_3 in H_2O, ≥ 99.99 % trace metals basis, Sigma-Aldrich), Nickel nitrate hexahydrate ($Ni(NO_3)_2.6H_2O$, 99.999 % trace metals basis, Sigma-Aldrich), Calcium nitrate tetrahydrate ($Ca(NO_3)_2 \cdot 4H_2O$, ≥ 99.0 %, Sigma-Aldrich), Magnesium nitrate hexahydrate ($Mg(NO_3)_2 \cdot 6H_2O$, ACS reagent, 99 %), Potassium nitrate (KNO_3, ReagentPlus®, ≥ 99.0 %, Sigma-Aldrich), Cerium(III) nitrate hexahydrate ($Ce(NO_3)_3 \cdot 6H_2O$, 99.999 % trace metals basis, Sigma-Aldrich) and distilled water are used as starting materials.

The catalysts were prepared according to the sol-gel aqueous method used in [40–42]. The alumina hydroxide sol was produced and washed twice with water. $Ni(NO_3)_2$ was added, followed by the addition of dopants. Doping was performed with the corresponding nitrate salts (with Ca, Ce, Mg or K nitrates). After salt additions, the sol was stirred for 30 min and dried for 24 h at 85 °C under 700 mbar, then for 24 h at 110 °C under 900 mbar. Finally, the dried samples were calcined under air for 5 h at 550 °C with a heating rate of 2 °C/min.

Simple doped catalysts were composed of γ-Al_2O_3, with 10 wt. % of Ni, and 1.5 wt. % of elements which were in the form of oxide (*i.e.* Ca, Ce, K, Mg).

Doping with 3 wt. % of the best oxides (*i.e.* Ca, K) and double doping (1.5 wt. % of two different oxides) were also synthesized.

The amount of reagents were denoted in Supplementary Materials in Table S1.

2.2. Characterization

Sample compositions were determined by inductively coupled plasma–atomic emission spectroscopy (ICP–AES), equipped with an ICAP 6500 THERMO Scientific device [41,42].

Textural properties were evaluated thanks to nitrogen adsorption-desorption isotherms which are measured at -196 °C on a Micromeretics ASAP 2010 instrument [41,42]. The microporous volume, V_{DR}, was calculated by the Dubinin-Raduskevitch theory. The pore size distributions was determined by the Broekhoff de Boer method (BdB) [42,43].

The crystallinity of the samples were measured by X-ray diffraction with a diffractometer Siemens D5000 (Cu-K_α radiation) between 30° and 80° (2θ) with a step time of 18 s and a step size of 0.04 s [41,42]. The alumina and $Ni^{(0)}$ crystallites sizes were calculated by using the Scherrer equation centered on the (4 0 0) ray (2θ = 67.0°) and on the (2 0 0) ray (2θ = 51.83°) respectively [41,42]. The same calculation was performed on all other characteristic peaks of Ni and alumina, no difference was observed.

The sizes of metallic particles and their distribution are measured by transmission electron microscopy (TEM) performed on a CM10-PW6020 Philips Electron Microscope by averaging the measurement of approximately 100 particles on TEM micrographs with the TEM software [41,42].

H_2 reduction steps were performed on 1 g of sample. The reactor was first purged with helium at room temperature (15 min, 50 mL/min) [41,42]. Then, a hydrogen flux was sent to the sample (50 mL/min) and the temperature was increased (from 25 °C to 750 °C with a heating rate of 5 °C/min) [41,42]. After 1 h at 750 °C, the heating was stopped and the reactor was purged with helium (50 mL/min).

Temperature Programmed Reduction measurements were performed with a TPD/R/O 1100 device from CE instruments to give information about the reduction of the metallic species (*i.e.* Ni) present in the samples [41,42].

The surface acidity measurements were obtained on a Temperature Programmed Desorption (TPD) performed on an AutoChem II 2920 instrument from Micromeretics. The measurements were performed according to the following steps: first, the samples were heated from 25 °C to 600 °C with a heating rate of 10 °C/min and under an air flow of 50 mL/min. These conditions were maintained for 1 h at 600 °C. Then, the samples were purged with a He flow of 50 mL/min and the heating was stopped until the temperature reached 100 °C. At 100 °C, an ammonia gas mixture (5 % vol. NH_3/95 %vol. He) was injected with a flow-rate of 50 mL/min during 1 h. Thereafter, the sample was purged once more with 50 mL/min of He for 30 min. Finally, a slow heating rate was applied (2 °C/min, 100-600 °C) under He (50 mL/min). The TPD-NH_3 curves were determined from this last operating step. The amount of ammonia by gram of catalysts (V_{NH3}, $mmol_{NH3}/g$) desorbed during the TPD-NH_3 measurements were determined by comparing the area under the peaks with a calibration performed on the instrument.

After the catalytic tests, carbon deposits are studied with thermogravimetric (TG) and differential scanning calorimetry (DSC) measurements, which are realized with a Sensys Setaram instrument [41,42]. Samples are heated from 25 to 800 °C with a heating rate of 2 °C/min under air (20 mL/min).

2.3. Catalytic experiments

The samples are tested at 650 °C, for 300 min, with a standard procedure described in [40,42,44], with a toluene concentration of 24,000 ppmv and a gas mixture of 31.5 %vol. H_2, 31.5 %vol. CO, 15.2 %vol. CO_2, 11 %vol. H_2O, and 10 %vol. CH_4. The mass of the catalyst is set to 300 mg, for a catalytic bed height of 12 mm, with a gas flowrate of 50 mL/min and consequently a *GHSV* of 5000 h^{-1} (residence time of 0.72 s) [41,42].

All the equations to calculate the toluene conversion (C_T), the benzene selectivity (S_B), the methane conversion, (C_{CH4}), the consumption rate of toluene, (r_T) and the coke tendency (*Coke**) are fully detailed in [41,42].

3. Results and Discussion

3.1. Catalysts doped with 1.5 wt. % of oxide

3.1.1. Composition and textural properties

Table 1 shows the composition and textural properties of 10 wt. % Ni/γ-Al_2O_3 catalysts prepared with 1.5 wt. % of oxide. The theoretical and actual loadings were similar for all samples. All the samples were micro- and mesoporous with S_{BET}, V_p and V_{DR} values similar for all the samples (an example of isotherm is presented in Figure S1 for 10Ni-Ca1.5 sample in the Supplementary Materials). It seems that, at these loadings, the element doping had no visible influence on the textural properties of the samples. Consequently, it was assumed that the differences in catalytic performances exhibited were only attributed to the different dopants.

3.1.2. TPR and NH_3-TPD measurements of Ni/γ-Al_2O_3 catalysts doped with 1.5 wt. % of oxide

Figure 1 shows the TPR profile of 10 wt. % Ni/γ-Al_2O_3 catalysts doped with 1.5 wt. % of oxide. The metallic nickel particle sizes obtained by TEM and XRD measurements (Figure 2 and 3) after TPR measurements are presented in Table 2. The TPR profiles of samples 10Ni-1.5Ca and 10Ni-1.5K (Figure 1) showed a peak with low intensity located around 500 °C, which could be attributed to nickel oxide with low interactions with the alumina support. Indeed, in previous studies [45], it was shown that the strong affinity of CaO or K_2O with Al_2O_3 can partially decrease the interactions between Ni and γ-Al_2O_3. However, the main reduction peak of Ni stayed at the same temperature (around 850 °C) compared to sample 10Ni.

For sample 10Ni-1.5Mg (Figure 1), the addition of magnesium shifted the reduction step of Ni towards higher temperatures (ΔT = + 75 °C) compared to sample 10Ni. This influence of MgO on the nickel reduction has been well established in the literature [30,46,47]. According to Wang *et al.* [23], "*because MgO has a lattice parameter and bond distance close to those of NiO, MgO and NiO can form a solid solution resulting in its lowered reducibility*". However, contrary to the results seen in some previous studies [46,48], sample 10Ni-1.5Mg did not show smaller metallic nickel particles after TPR (d_{XRD} = 25 nm and d_{TEM} = 34 nm) compared to other samples (Table 2).

Sample 10Ni-1.5Ce presented a TPR profile (Figure 1) with a broad peak of low intensity located between 450 °C and 700 °C, which was attributed to the $CeO_2 \rightarrow Ce_2O_3$ reduction step [49,50]. The main reduction peak of Ni was shifted towards higher temperatures (ΔT = + 65 °C) compared to sample 10Ni. Despite the fact that the interactions between Ni and CeO_x were strong, the consequence of CeO_2 on the reducibility of Ni supported on γ-Al_2O_3 varies among the publications. Some authors found that the addition of cerium decreased the temperature needed for the reduction of Ni [33,51]. This was attributed to Ni-CeO_x interactions, which might prevent the formation of $NiAl_2O_4$ spinel, a difficult phase to reduce. In contrary, Liu *et al.* [50] found that the addition of Ce made the reduction of Ni oxides more difficult. The author attributed the delay of the reduction to the presence of CeO_x species on the surface of Ni. In this work, whereas the addition of CeO_2 apparently allowed a decrease in the sintering rate of the $Ni^{(0)}$ particles [33,50,52], sample 10Ni-1.5Ce presented larger metallic particle sizes after TPR (d_{XRD} = 28 nm and d_{TEM} = 44 nm) compared to the other samples (Table 2). This could be a consequence of the interactions of Ni-CeO_x as above [33,51].

Figure 2 presents TEM micrographs for the four samples doped with 1.5 wt. % of oxide after TPR measurements. All samples had similar aspects (highly dispersed Ni metallic nanoparticles into alumina matrix) with variation in the Ni nanoparticles size only (Table 2).

Concerning the XRD, all samples are represented on Figure 3. They presented similar patterns with peaks of Ni and γ-Al_2O_3. No shift in peak position is observed. The Ni crystallite size was in the same range for all samples doped with 1.5 wt. % of oxide (*i.e.* 23 to 28 nm).

NH_3-TPD measurements (Figure 4) and their corresponding volumes of NH_3 desorbed (Table 2) led to very close results for all samples doped with 1.5 wt. % of oxide. The presence of similar acido-basicity properties was attributed to the low amount of alkali and to the relatively low calcination temperature (550 °C), which was insufficient to enable the formation of strong interactions between the alkali and the γ-Al_2O_3 support during the preparation of catalysts [53–55].

3.1.3. Catalytic performances of Ni/γ-Al_2O_3 catalysts doped with 1.5 wt. % of oxide

The catalytic performances of all samples doped with 1.5 wt. % of oxide were measured. Figures 5a and 5b show the toluene conversion, C_T, as a function of time and the toluene reforming rate, r_T, as a function of the amount of carbon deposit. Figures 5c and 5d show the benzene selectivity, S_B, and the methane conversion, C_{CH4}. Figure 6 shows the DSC curves under air performed on samples after catalytic tests. The metallic particle sizes, the type of metallic phase present after tests as well as the catalytic performances of the samples are resumed in Table 3.

The materials doped with an alkali (*i.e.* samples 10Ni-1.5Ca, 10Ni-1.5Mg, and 10Ni-1.5K) showed much lower S_B values (4-9 %, instead of 15 % for sample 10Ni) and lower amounts of carbon deposit after test (*Coke* of 0.06-0.08 g_{Carbon}/g_{Cata}, instead of 0.10 g_{Carbon}/g_{Cata} for sample 10Ni) (Table 3). Furthermore, samples 10Ni-1.5Ca and 10Ni-1.5K did not show any filamentous carbon after the catalytic test because only one large peak located between 350 °C and 550 °C, characteristic of amorphous carbon combustion, is present on DSC curves (Figure 6). Taking into account that the TPD-NH_3 measurements (Figure 4 and Table 2) revealed that

the alkali addition did not have a strong influence on the acidity of the alumina supports, it was assumed that the better anti-coking properties showed by the alkali-doped samples were mostly due to their better ability to adsorb and dissociate the H_2O and CO_2 molecules [56]. In this way, the higher presence of oxidative species (O^* and HO^*) favored the gasification of the carbonaceous compounds produced during the cracking of the toluene and prevented these molecules to react with each other and to form stable filamentous carbon [3,57,58].

Figures 5a and 5b revealed that sample 10Ni-1.5Mg presented a very low C_T value at the beginning of the catalytic test and that a longer period was required to activate this sample during the test. Furthermore, this sample showed low C_T values throughout the whole duration of the test (at 300 min for sample 10Ni-1.5Mg, C_T = 31 %, whereas C_T = 51 % for sample 10Ni). Hence, in that case, too strong NiO-MgO interactions (see TPR curves, Figure 1) were detrimental for the catalytic activity. Moreover, the formation of filamentous carbon and lowest reaction rate were observed. It was supposed that the active phase was not well adapted for the reaction and as the reaction was slower, more intermediate product as benzene were formed.

Sample 10Ni-1.5Ca showed slightly lower C_T and C_{CH4} values (Table 3) compared to sample 10Ni. It was assumed that these lower conversion values were caused by the covering of the $Ni^{(0)}$ particles by CaO. Indeed, during catalytic tests, alkali oxides could migrate and cover the surface of the $Ni^{(0)}$ particles. This covering could have beneficial influences because it favors the adsorption-dissociation of H_2O and CO_2 molecules, and therefore increases the direct oxidation of the carbonaceous species cracked [24,59–61]. However, for the steam and dry reforming of CH_4, the presence of alkali at the surface of $Ni^{(0)}$ could also block the access to some active sites and slightly decrease the catalytic activity of the materials. This effect depended on different parameters such as the synthesis method [62,63] or the amount of alkali doping [64]. Furthermore, the alkali element could modify the electronic environment of the Ni atoms and hence increase the energetic barrier needed for the CH_4 dissociation [24,65].

Despite a very slight decrease in the C_{CH4} value (Table 3), the addition of potassium presented beneficial influences on the catalytic performances of sample 10Ni-1.5K compared to sample 10Ni: lower S_B value (4 %), higher r_T value (7.2 .10^{-2} $mol_{Tolu}/(g_{Ni}.h)$), and low amount of carbon deposit after test (*Coke* = 0.08 g_{Carbon}/g_{Cata}) (Table 3). No clear explanation was found in the literature to explain the differences in activities between K and Ca doped materials. An explanation of these differences could be the higher lability of K^+ ions compared to Ca^{2+} ions, as a consequence of higher rates of adsorption-dissociation of H_2O and CO_2 molecules for sample 10Ni-1.5K.

Despite the fact that the addition of cerium in the composition of reforming catalysts is more and more encouraged in the literature [17,66–68], sample 10Ni-1.5Ce did not show exceptional performances. Indeed, sample 10Ni-1.5Ce showed similar catalytic activity and similar coking values as reference sample 10Ni (Table 3). The low influences of the Ce doping could be attributed to inadequate interactions between the γ-Al_2O_3 support and the Ce oxide species. Indeed, in contrary to the present aqueous sol-gel synthesis used, in most previous studies, the supports were prepared by the doping of commercial γ-Al_2O_3 support with Ce by incipient wetness methods [22,33,69,70]. In these studies, the calcination temperature varied from 450 °C to 1200 °C. This strong influence of the preparation method on the properties of Ni/CeO_2/Al_2O_3 catalysts was notably highlighted by Tomishige *et al.* [71], who showed that catalysts prepared by co-impregnation method exhibited much higher performances than the same materials prepared by sequential impregnation. In the present case, it was assumed that the calcination temperature was not high enough to create sufficient interactions between the Ce oxide species and alumina, and to form the anti-coking $AlCeO_x$ phases.

3.2. Catalysts doped with two oxides

10 wt. % Ni/γ-Al_2O_3 catalysts doped with 1.5 wt. % of one oxide and 1.5 wt. % of a second oxide (*i.e.* Oxide = Ce, Ca, Mg or K) were synthesized, characterized, and tested for the

reforming of 24,000 ppmv of toluene at 650 °C. Figure 7a gives an overview of the reforming rate of toluene, r_T, as a function of the amount of carbon deposit after test for all samples. Figures 7b and 7c give an overview of the benzene selectivity, S_B, and methane conversion, C_{CH4}, for all catalysts doped with two oxides.

It appeared that samples 10Ni-1.5Ca-1.5K and 10Ni-1.5Ce-1.5K showed the best catalytic performances. Hence, the properties and catalytic performances of both best catalysts are presented in the following parts.

3.2.1. Composition, crystallinity, particle size and reducibility of samples doped with Ca+K or Ce+K

For samples 10Ni-1.5Ca-1.5K and 10Ni-1.5Ce-1.5K, the theoretical and actual compositions are similar (Table 1).

Figure 8 shows the TPR profiles of samples 10Ni-1.5Ca-1.5K and 10Ni-1.5Ce-1.5K. For a better comparison, the curves of samples 10Ni-1.5Ca, 10Ni-1.5K, 10Ni-1.5Ce, and 10Ni were also added in Figure 8. Similarly, as for samples 10Ni-1.5Ca and 10Ni-1.5K, sample 10Ni-1.5Ca-1.5K showed a small and broad peak located between 450 °C and 625 °C, attributed to the presence of Ca and K which reduce the interactions between Ni and γ-Al_2O_3 [45,72]. Furthermore, sample 10Ni-1.5Ca-1.5K did not show a shift of the Ni reduction peak. For sample 10Ni-1.5Ce-1.5K, as for sample 10Ni-1.5K, a peak of very low intensity was also observed between 400 °C and 600 °C (Figure 8). Furthermore, the peak of Ni reduction at 850 °C was broadened and shifted towards higher temperatures, which highlighted the presence of strong Ni-CeO_x interactions.

Samples 10Ni-1.5Ca-1.5K and 10Ni-1.5Ce-1.5K presented similar Ni particle sizes measured after TPR measurements (Table 2), their XRD patterns were similar to those of Figure 3. It was also observed that sample 10Ni-1.5Ce-1.5K present lower Ni particle sizes (d_{TEM} = 33

nm and d_{XRD} = 25 nm, TEM on Figure 2e) compared to sample 10Ni-1.5Ce (d_{TEM} = 44 nm and d_{XRD} = 28 nm, TEM on Figure 2d) (Table 2).

3.2.2. Catalytic performances of samples doped with Ca+K or Ce+K

Figure 9 shows the toluene conversion, C_T, as a function of time and the toluene reforming rate, r_T, as a function of the amount of carbon deposit for samples 10Ni-1.5Ca-1.5K, 10Ni-1.5Ce-1.5K, the single doped catalysts (*i.e.* samples 10Ni-1.5Ce, 10Ni-1.5Ca, and 10Ni-1.5K), and reference 10Ni. Figure 10 shows the DSC curves under air realized after catalytic tests. The $Ni^{(0)}$ particle sizes and the catalytic performances of the samples are shown in Table 3.

In Figure 9 and Table 3, sample 10Ni-1.5Ca-1.5K evidenced that under these conditions of catalytic test, the combination of Ca and K led to a catalyst that showed a slightly higher amount of carbon deposit (Coke = 0.09 g_{Carbon}/g_{Cata}), but a higher r_T value (8.6 $.10^{-2}$ $mol_{Tolu}/(g_{Ni}.h)$) compared to samples 10Ni-1.5Ca and 10Ni-1.5K. A synergistic effect between Ca and K could increase the adsorption-dissociation of H_2O and CO_2 molecules [58,73]. Furthermore, the better catalytic activity observed for sample 10Ni-1.5Ca-1.5K could also be attributed to the increase of reducibility of the nickel oxide caused by the presence of alkali (Figure 8). Finally, as for samples 10Ni-1.5Ca and 10Ni-1.5K, the carbon deposit of sample 10Ni-1.5Ca-1.5K was only constituted of amorphous carbon.

Though the association of Ce and K did not show the expected anti-coking effect, sample 10Ni-1.5Ce-1.5K showed a higher catalytic activity compared to samples 10Ni-1.5Ce and 10Ni-1.5K. Indeed, in Figure 9 and Table 3, sample 10Ni-1.5Ce-1.5K showed the highest r_T value of all the samples of this study (1.1 $.10^{-1}$ $mol_{Tolu}/(g_{Ni}.h)$) for an acceptable amount of carbon deposit (*Coke* = 0.11 g_{Carbon}/g_{Cata}).

3.3. Influences of oxide dopant loading

In view of the results obtained in the upper parts of this study, it was decided to study 10 wt. % Ni/γ-Al_2O_3 catalysts doped with a higher loading (*i.e.* 3 wt. %) of Ca or K. Table 1 shows that the theoretical and actual compositions of these samples are very similar.

3.3.1. Crystallinity, particle size and reducibility of samples doped with 3 wt. % of Ca or K

Figure 11 shows the TPR profiles of the samples doped with different loadings of Ca or K. The metallic nickel particle sizes after TPR measurements determined by TEM and XRD analyses are presented in Table 2, the TEM picture for sample 10Ni-3K is presented on Figure 2f. The XRD patterns were identical to the corresponding sample doped with 1.5 wt. % (Figure 3).

Like sample 10Ni-1.5Ca, sample 10Ni-3Ca showed a small peak of H_2 consumption located at about 500 °C (Figure 11). However, the higher doping of Ca shifted the main peak of Ni reduction towards higher temperatures (ΔT = + 70°C). Indeed, when added in important amounts, CaO can cover the NiO particles and therefore decrease their reducibility [64]. After TPR measurements, sample 10Ni-3Ca presented similar metallic Ni particle sizes compared to sample 10Ni-1.5Ca (Table 2).

The TPR profile of sample 10Ni-3K also presented a small H_2 consumption peak located around 500 °C. Similarly to sample doped with Ca, the addition of 3 wt. % of K led to a shift of the Ni reduction peak towards higher temperatures (ΔT = + 75 °C) (Figure 11), probably for the same reason explained for sample 10Ni-3Ca. Sample 10Ni-3K presented similar metallic Ni particles size compared to sample 10Ni-3Ca after TPR measurements (Table 2). No difference in TEM picture was observed with higher loading (Figure 2), only the Ni particle size could vary a little bit between samples.

3.3.2. Catalytic experiments on samples doped with 3 wt. % of Ca or K

Figure 12 shows the toluene conversion, C_T, as a function of time and the toluene reforming rate, r_T, as a function of carbon deposit for the samples prepared with different loadings of Ca or K. Figure 13 shows the DSC curves under air performed on samples after catalytic tests. The metallic Ni particle sizes after test determined by TEM and XRD measurements, as well as the catalytic performances are listed in Table 3.

Sample 10Ni-3Ca presented a lower r_T value (3.9 $.10^{-2}$ $mol_{Tolu}/(g_{Ni}.h)$) and a lower C_{CH4} value (3 %) compared to sample 10Ni-1.5Ca (Table 3). These lower catalytic activity values were attributed to the lower reducibility of nickel in sample 10Ni-3Ca (see TPR in Figure 11) and probably also to the blockage of $Ni^{(0)}$ active sites by the large amount of CaO present in the sample. Despite a lower catalytic activity, sample 10Ni-3Ca presented the same amount of carbon deposit as sample 10Ni-1.5Ca (0.07 g_{Carbon}/g_{Cata}). Furthermore, whereas sample 10Ni-1.5Ca presented carbon deposit only constituted of amorphous carbon, the increase of the loading of Ca up to 3 wt. % led to the formation of filamentous carbon because a peak around 590 °C, characteristic of combustion of structured carbon, is present in Figure 13. In this way, whereas after TPR measurements, samples 10Ni-1.5Ca and 10Ni-3Ca presented similar Ni particle sizes (Table 2), after catalytic test, sample 10Ni-3Ca presented in contrary larger Ni particles (d_{XRD} = 19 nm and d_{TEM} = 15 nm) with a broad size distribution (σ_{TEM} = 17 nm) (Table 3). This presence of larger Ni particles could explain the growth of filamentous carbon. Indeed, it has been shown in previous studies that the alkali improves the sintering rate of Ni particles because the higher loading of Ca increases the formation of more mobile $Ca(OH)_2$ and $CaCO_3$ species during the catalytic test [24,74–76].

Sample 10Ni-3K also presented lower r_T and C_{CH4} values. The reason was attributed to a large covering of the $Ni^{(0)}$ particles by K_2O [62,65,77]. However, in this study, the catalytic activity was only very slightly decreased, whereas in previous studies concerning methane reforming, the catalytic activity was strongly decreased because of the presence of K [78]. It

was assumed that the high covering of the metallic Ni particle by K_2O allowed in contrary to efficiently prevent the catalyst from the formation of carbon deposit (*Coke* = 0.02 g_{Carbon}/g_{Cata}). As for sample 10Ni-3Ca, sample 10Ni-3K was more sensitive towards sintering during the catalytic test (d_{XRD} = 17 nm, d_{TEM} = 13 nm, and σ_{TEM} = 14 nm, Table 3), due to a higher loading of K. However, no filamentous carbon was observed after the test for 10Ni-3K probably due to the anti-coking ability of K (Figure 13).

Hence, catalysts with a higher loading of alkali (*i.e.* Ca or K) presented lower catalytic activity and metallic nickel particles are more inclined to sinter. However, the good anti-coking performance of K_2O countered the drawbacks caused by the presence of larger Ni particles and allowed keeping a sample almost free of carbon after 5 h of catalytic test at 650 °C.

4. Conclusions

In this study, the physico-chemical properties and catalytic activity of 10 wt. % Ni/γ-Al_2O_3 catalyst doped with different oxides were studied. Twelve doped Ni/γ-Al_2O_3 catalysts were synthesized by sol-gel process. One Ni/γ-Al_2O_3 catalyst without dopant was also synthesized as reference material.

NH_3-TPD measurements highlighted that the addition of 1.5 wt. % of alkali (*i.e.* Ca, K or Mg) did not influence the acido-basicity properties of 10 wt. % Ni/γ-Al_2O_3 catalysts. It was assumed that no sufficient interactions were formed between the oxides and the alumina support during the preparation of the catalysts.

All samples doped with 1.5 wt. % of oxide (*i.e.* Ca, K, Mg or Ce) presented a decrease of benzene selectivity and of the amount of carbon deposit. These results were attributed to a better degradation of the intermediate compounds of toluene and of the carbonaceous compounds because of a higher amount of H_2O and CO_2 molecules adsorbed on these oxides. The addition of Mg led to strong Ni/MgO interactions that decreased the catalytic activity of the catalyst at

650 °C and increased the filamentous carbon formation. The catalyst doped with 1.5 wt. % of Ce did not show the remarkable anti-coking properties that were expected in literature at 650 °C. This was attributed to the synthesis method by sol-gel process, whose calcination temperature was believed to be insufficient to form $AlCeO_x$ phase. The addition of 1.5 wt. % of Ca led to a slightly lower catalytic activity at 650 °C, but to a better resistance against coking. However, when the loading of Ca increased up to 3 wt. %, the sample showed a harder Ni reducibility, which led to a lower catalytic activity during the catalytic test at 650 °C. Furthermore, because of this large amount of Ca, the sintering of the $Ni^{(0)}$ particles was favored during the catalytic test, which resulted in an increase of the formation of filamentous carbon. Potassium appeared to be the most interesting alkali dopant. Indeed, the catalyst doped with 1.5 wt. % of K showed a very good toluene reforming activity (around 55 % of toluene conversion) associated to a low amount of carbon deposit. At higher doping (*i.e.* 3 wt. %), the sample showed a slight decrease of its catalytic activity and a low methane conversion during the catalytic test at 650 °C. Once more, this was attributed to the covering of the $Ni^{(0)}$ particles by K_2O. The high amount of alkali increased the sintering of the $Ni^{(0)}$ particles and led to the formation of large metallic particles with a broad size distribution. However, despite the presence of large $Ni^{(0)}$ particles, the sample doped with 3 wt. % of K showed almost no carbon deposit after the catalytic test at 650 °C.

Among the different compositions of Ni/γ-Al_2O_3 catalysts doped with different types of oxides, the catalysts doped either with K+Ce, or K+Ca showed the most interesting performances. At 650 °C, the sample doped with K+Ce showed the highest toluene reforming rate among all catalysts of this study (with a toluene conversion of 70 %). However, it was assumed that at these temperatures, the gasification rates of the carbonaceous compounds were insufficient to balance the high rate of toluene cracking, which resulted in large amounts of carbon deposits. In contrary, the sample doped with K+Ca showed interesting toluene and

methane conversions, associated to a relatively low amount of carbon deposit exclusively formed of amorphous type. Furthermore, in spite of its high loading of alkali, this catalyst still presented small $Ni^{(0)}$ particles around 10 nm with a narrow size distribution. Therefore, it was shown that catalysts with very interesting catalytic activity and good anti-coking performances can be obtained only thanks to the combination of classic alkali dopant (*i.e.* Ca and K) and without the use of the expensive ceria element.

Acknowledgements

V. Claude thanks to F.R.S.-F.N.R.S. for his doctoral grant obtained with the "Fonds de Recherche collective" n° 2.4541.12. S. D. L. is also grateful to F.R.S.-F.N.R.S for her Senior Research Associate position. R. G. T. benefits from funding of F.R.S.-FNRS under a Fund for Research Training in Industry and Agriculture (FRIA) grant. The authors also acknowledge the Ministère de la Région Wallonne Direction Générale des Technologies, de la Recherche et de l'Energie (DG06) and the Fond de Bay for financial supports.

Compliance with ethical standards

Conflict of interest: The authors declare that they have no conflicts of interest.

Data availability

The raw/processed data required to reproduce these findings cannot be shared at this time as the data also forms part of an ongoing study.

References

[1] V. Claude, C. Courson, M. Köhler, S.D. Lambert, Overview and Essentials of Biomass Gasification Technologies and Their Catalytic Cleaning Methods, Energy and Fuels. 30 (2016) 8791–8814. doi:10.1021/acs.energyfuels.6b01642.

[2] V. Claude, C. Courson, M. Köhler, S.D. Lambert, Correction to overview and

essentials of biomass gasification technologies and their catalytic cleaning methods (Energy Fuels (2016) 30:11 (8791-8814) DOI: 10.1021/acs.energyfuels.6b01642), Energy and Fuels. 31 (2017) 1050. doi:10.1021/acs.energyfuels.6b03436.

[3] F.L. Chan, A. Tanksale, Review of recent developments in Ni-based catalysts for biomass gasification, Renew. Sustain. Energy Rev. 38 (2014) 428–438. doi:10.1016/j.rser.2014.06.011.

[4] M. Qiu, Y. Li, T. Wang, Q. Zhang, C. Wang, X. Zhang, et al., Upgrading biomass fuel gas by reforming over Ni–MgO/γ-Al2O3 cordierite monolithic catalysts in the lab-scale reactor and pilot-scale multi-tube reformer, Appl. Energy. 90 (2012) 3–10. doi:10.1016/j.apenergy.2011.01.064.

[5] F. Davar, M. Salavati-Niasari, N. Mir, K. Saberyan, M. Monemzadeh, E. Ahmadi, Thermal decomposition route for synthesis of Mn3O4 nanoparticles in presence of a novel precursor, Polyhedron. 29 (2010) 1747–1753. doi:10.1016/j.poly.2010.02.026.

[6] F. Motahari, M.R. Mozdianfard, F. Soofivand, M. Salavati-Niasari, NiO nanostructures: Synthesis, characterization and photocatalyst application in dye wastewater treatment, RSC Adv. 4 (2014) 27654–27660. doi:10.1039/c4ra02697g.

[7] F. Mohandes, F. Davar, M. Salavati-Niasari, Magnesium oxide nanocrystals via thermal decomposition of magnesium oxalate, J. Phys. Chem. Solids. 71 (2010) 1623–1628. doi:10.1016/j.jpcs.2010.08.014.

[8] T. Gholami, M. Salavati-Niasari, Effects of copper:aluminum ratio in CuO/Al2O3 nanocomposite: Electrochemical hydrogen storage capacity, band gap and morphology, Int. J. Hydrogen Energy. 41 (2016) 15141–15148. doi:10.1016/j.ijhydene.2016.06.191.

[9] M. Salavati-Niasari, Synthesis and characterization of host (nanodimensional pores of

zeolite- Y)-guest [unsaturated 16-membered octaaza-macrocycle manganese(II), cobalt(II), nickel(II), copper(II), and zinc(II) complexes] nanocomposite materials, Chem. Lett. 34 (2005) 1444–1445. doi:10.1246/cl.2005.1444.

[10] M. Salavati-Niasari, Host (nanocavity of zeolite-Y)-guest (tetraaza[14]annulene copper(II) complexes) nanocomposite materials: Synthesis, characterization and liquid phase oxidation of benzyl alcohol, J. Mol. Catal. A Chem. 245 (2006) 192–199. doi:10.1016/j.molcata.2005.09.046.

[11] M. Salavati-Niasari, Ship-in-a-bottle synthesis, characterization and catalytic oxidation of styrene by host (nanopores of zeolite-Y)/guest ([bis(2-hydroxyanil)acetylacetonato manganese(III)]) nanocomposite materials (HGNM), Microporous Mesoporous Mater. 95 (2006) 248–256. doi:10.1016/j.micromeso.2006.05.025.

[12] M. Salavati-Niasari, M. Shaterian, M.R. Ganjali, P. Norouzi, Oxidation of cyclohexene with tert-butylhydroperoxide catalysted by host (nanocavity of zeolite-Y)/guest (Mn(II), Co(II), Ni(II) and Cu(II) complexes of N,N′-bis(salicylidene)phenylene-1,3-diamine) nanocomposite materials (HGNM), J. Mol. Catal. A Chem. 261 (2007) 147–155. doi:10.1016/j.molcata.2006.07.048.

[13] M. Salavati-Niasari, M.R. Loghman-Estarki, F. Davar, Controllable synthesis of nanocrystalline CdS with different morphologies by hydrothermal process in the presence of thioglycolic acid, Chem. Eng. J. 145 (2008) 346–350. doi:10.1016/j.cej.2008.08.040.

[14] M. Mousavi-Kamazani, Z. Zarghami, M. Salavati-Niasari, Facile and Novel Chemical Synthesis, Characterization, and Formation Mechanism of Copper Sulfide (Cu2S, Cu2S/CuS, CuS) Nanostructures for Increasing the Efficiency of Solar Cells, J. Phys. Chem. C. 120 (2016) 2096–2108. doi:10.1021/acs.jpcc.5b11566.

[15] M. Sabet, M. Salavati-Niasari, O. Amiri, Using different chemical methods for deposition of CdS on TiO2 surface and investigation of their influences on the dye-sensitized solar cell performance, Electrochim. Acta. 117 (2014) 504–520. doi:10.1016/j.electacta.2013.11.176.

[16] S. Anis, Z. a. Zainal, Tar reduction in biomass producer gas via mechanical, catalytic and thermal methods: A review, Renew. Sustain. Energy Rev. 15 (2011) 2355–2377. doi:10.1016/j.rser.2011.02.018.

[17] D. Li, Y. Nakagawa, K. Tomishige, Development of Ni-Based Catalysts for Steam Reforming of Tar Derived from Biomass Pyrolysis, Chinese J. Catal. 33 (2012) 583–594. doi:10.1016/S1872-2067(11)60359-8.

[18] D. Świerczyński, S. Libs, C. Courson, a. Kiennemann, Steam reforming of tar from a biomass gasification process over Ni/olivine catalyst using toluene as a model compound, Appl. Catal. B Environ. 74 (2007) 211–222. doi:10.1016/j.apcatb.2007.01.017.

[19] J.N. Kuhn, Z. Zhao, A. Senefeld-Naber, L.G. Felix, R.B. Slimane, C.W. Choi, et al., Ni-olivine catalysts prepared by thermal impregnation: Structure, steam reforming activity, and stability, Appl. Catal. A Gen. 341 (2008) 43–49. doi:10.1016/j.apcata.2007.12.037.

[20] Z. Zhao, N. Lakshminarayanan, J.N. Kuhn, A. Senefeld-Naber, L.G. Felix, R.B. Slimane, et al., Optimization of thermally impregnated Ni–olivine catalysts for tar removal, Appl. Catal. A Gen. 363 (2009) 64–72. doi:10.1016/j.apcata.2009.04.042.

[21] M.M. Yung, W.S. Jablonski, K. a. Magrini-Bair, Review of Catalytic Conditioning of Biomass-Derived Syngas, Energy & Fuels. 23 (2009) 1874–1887.

[22] Z.R. Ismagilov, M.A. Kerzhentsev, V.A. Sazonov, L.T. Tsykoza, N. V Shikina, V. V Kuznetsov, et al., Study of Catalysts for Catalytic Burners for Fuel Cell Power Plant Reformers, Korean J.Chem Eng. 20 (2003) 461–467.

[23] S. Wang, CO2 reforming of methane on Ni catalysts: Effects of the support phase and preparation technique, Appl. Catal. B Environ. 16 (1998) 269–277.

[24] J. Rostrup-Nielsen, Catalytic Steam Reforming, Catal. Sci. Technol. 5 (1984) 1–117. doi:doi.org/10.1007/978-3-642-93247-2_1.

[25] I. Zamboni, C. Courson, D. Niznansky, a. Kiennemann, Simultaneous catalytic H2 production and CO2 capture in steam reforming of toluene as tar model compound from biomass gasification, Appl. Catal. B Environ. 145 (2014) 63–72. doi:10.1016/j.apcatb.2013.02.046.

[26] S. Nwamaka-Ude, The Synthesis and Crystal Chemistry of Ca12Al14O33 doped with Fe2O3, Master's Thesis, University of Tennesse, 2010.

[27] C. Li, D. Hirabayashi, K. Suzuki, A crucial role of O2− and O22− on mayenite structure for biomass tar steam reforming over Ni/Ca12Al14O33, Appl. Catal. B Environ. 88 (2009) 351–360. doi:10.1016/j.apcatb.2008.11.004.

[28] S. Zhou, Y. Zhou, Y. Zhang, X. Sheng, Z. Zhang, J. Kong, Synthesis of core–shell-structured SBA-15@MgAl2O4 with enhanced catalytic performance of propane dehydrogenation, J. Mater. Sci. 49 (2013) 1170–1178. doi:10.1007/s10853-013-7797-4.

[29] J. Li, T. Ikegami, J. Lee, T. Mori, Y. Yajima, Synthesis of Mg ± Al spinel powder via precipitation using ammonium bicarbonate as the precipitant, J. Eur. Ceram. Soc. 21 (2001) 139–148.

[30] L. Garcia, R. French, S. Czernik, E. Chornet, Catalytic steam reforming of bio-oils for the production of hydrogen: effects of catalyst composition, Appl. Catal. A Gen. 201 (2000) 225–239.

[31] S. Seok, Mn-Promoted Ni/Al2O3 Catalysts for Stable Carbon Dioxide Reforming of Methane, J. Catal. 209 (2002) 6–15. doi:10.1006/jcat.2002.3627.

[32] M.E. Gálvez, S. Ascaso, P. Stelmachowski, P. Legutko, a. Kotarba, R. Moliner, et al., Influence of the surface potassium species in Fe–K/Al2O3 catalysts on the soot oxidation activity in the presence of NOx, Appl. Catal. B Environ. 152–153 (2014) 88–98. doi:10.1016/j.apcatb.2014.01.041.

[33] S. Wang, G.Q. Lu, Role of CeO2 in Ni/CeO2-Al2O3 catalysts for carbon dioxide reforming of methane, Appl. Catal. B Environ. 19 (1998) 267–277. doi:10.1016/S0926-3373(98)00081-2.

[34] S. Lambert, C. Alié, J.P. Pirard, B. Heinrichs, Study of textural properties and nucleation phenomenon in Pd/SiO2, Ag/SiO2and Cu/SiO2cogelled xerogel catalysts, J. Non. Cryst. Solids. 342 (2004) 70–81. doi:10.1016/j.jnoncrysol.2004.06.005.

[35] L. Tasseroul, S.L. Pirard, S.D. Lambert, C. a. Páez, D. Poelman, J.P. Pirard, et al., Kinetic study of p-nitrophenol photodegradation with modified TiO 2 xerogels, Chem. Eng. J. 191 (2012) 441–450. doi:10.1016/j.cej.2012.02.050.

[36] J.G. Mahy, V. Claude, L. Sacco, S.D. Lambert, Ethylene polymerization and hydrodechlorination of 1,2-dichloroethane mediated by nickel (II) covalently anchored to silica xerogels, J. Sol-Gel Sci. Technol. 81 (2017) 59–68. doi:10.1007/s10971-016-4272-0.

[37] J.G. Mahy, C.A. Paez, C. Carcel, C. Bied, A.S. Tatton, C. Damblon, et al., Porphyrin-

based hybrid silica-titania as a visible-light photocatalyst, J. Photochem. Photobiol. A Chem. 373 (2019) 66–76. doi:10.1016/j.jphotochem.2019.01.001.

[38] M. Salavati-Niasari, M. Farhadi-Khouzani, F. Davar, Bright blue pigment CoAl2O4 nanocrystals prepared by modified sol-gel method, J. Sol-Gel Sci. Technol. 52 (2009) 321–327. doi:10.1007/s10971-009-2050-y.

[39] M. Salavati-Niasari, F. Davar, M. Farhadi, Synthesis and characterization of spinel-type CuAl2O4 nanocrystalline by modified sol-gel method, J. Sol-Gel Sci. Technol. 51 (2009) 48–52. doi:10.1007/s10971-009-1940-3.

[40] V. Claude, J.G. Mahy, J. Geens, C. Courson, S.D. Lambert, Synthesis of Ni/γ-Al2O3-SiO2 catalysts with different silicon precursors for the steam toluene reforming, Microporous Mesoporous Mater. 284 (2019) 304–315. doi:10.1016/j.micromeso.2019.04.027.

[41] V. Claude, J.G. Mahy, J. Geens, S.D. Lambert, Ni-doped γ-Al2O3 as secondary catalyst for bio-syngas purification: influence of Ni loading, catalyst preparation, and gas composition on catalytic activity, Mater. Today Chem. 13 (2019) 98–109. doi:10.1016/j.mtchem.2019.05.002.

[42] V. Claude, J.G. Mahy, R.G. Tilkin, S.D. Lambert, Enhancement of the catalytic performances and lifetime of Ni/<gamma>-Al2O3 catalysts for the steam toluene reforming via the combination of dopants: Inspection of Cu, Co, Fe, Mn and Mo species addition, Mater. Today Chem. 15 (2020) 100229.

[43] A.J. Lecloux, Texture of catalysts, Catal. Sci. Technol. 2 (1981) 171.

[44] V. Claude, J.G. Mahy, F. Micheli, J. Geens, S.D. Lambert, Sol-gel Ni/γ-Al2O3 material as secondary catalyst for toluene reforming: Tailoring the γ-Al2O3 substrate

with stearic acid, Microporous Mesoporous Mater. 291 (2020) 109681. doi:10.1016/j.micromeso.2019.109681.

[45] K.F.M. Elias, A.F. Lucrédio, E.M. Assaf, Effect of CaO addition on acid properties of Ni–Ca/Al2O3 catalysts applied to ethanol steam reforming, Int. J. Hydrogen Energy. 38 (2013) 4407–4417. doi:10.1016/j.ijhydene.2013.01.162.

[46] K. Nakamura, T. Miyazawa, T. Sakurai, T. Miyao, S. Naito, N. Begum, et al., Promoting effect of MgO addition to Pt/Ni/CeO2/Al2O3 in the steam gasification of biomass, Appl. Catal. B Environ. 86 (2009) 36–44. doi:10.1016/j.apcatb.2008.07.016.

[47] C. Wang, T. Wang, L. Ma, Y. Gao, C. Wu, Steam reforming of biomass raw fuel gas over NiO–MgO solid solution cordierite monolith catalyst, Energy Convers. Manag. 51 (2010) 446–451. doi:10.1016/j.enconman.2009.10.006.

[48] V.R. Choudhary, B.S. Uphade, A.S. Mamman, Oxidative Conversion of Methane to Syngas over Nickel Supported on Commercial Low Surface Area Porous Catalyst Carriers Precoated with Alkaline and Rare Earth Oxides, 293 (1997) 281–293.

[49] J. Nishikawa, K. Nakamura, M. Asadullah, T. Miyazawa, K. Kunimori, K. Tomishige, Catalytic performance of Ni/CeO2/Al2O3 modified with noble metals in steam gasification of biomass, Catal. Today. 131 (2008) 146–155. doi:10.1016/j.cattod.2007.10.066.

[50] Q. Liu, J. Gao, M. Zhang, H. Li, F. Gu, G. Xu, et al., Highly active and stable Ni/γ-Al 2O3 catalysts selectively deposited with CeO2 for CO methanation, RSC Adv. 4 (2014) 16094. doi:10.1039/C4RA00746H.

[51] T. Miyazawa, T. Kimura, J. Nishikawa, S. Kado, K. Kunimori, K. Tomishige, Catalytic performance of supported Ni catalysts in partial oxidation and steam reforming of tar

derived from the pyrolysis of wood biomass, Catal. Today. 115 (2006) 254–262. doi:10.1016/j.cattod.2006.02.055.

[52] K. Tapia-Parada, G. Valverde-Aguilar, A. Mantilla, M. a. Valenzuela, E. Hernández, Synthesis and characterization of Ni/Ce–SiO2 and Co/Ce–TiO2 catalysts for methane decomposition, Fuel. 110 (2013) 70–75. doi:10.1016/j.fuel.2012.11.022.

[53] M. Puchalska, E. Zych, M. Sobczyk, A. Watras, P. Deren, Effect of charge compensation on up-conversion and UV excited luminescence of Eu3+ in Yb3+-Eu3+ doped calcium aluminate CaAl4O7, Mater. Chem. Phys. 147 (2014) 304–310. doi:10.1016/j.matchemphys.2014.05.003.

[54] J.G. Li, T. Ikegami, J.H. Lee, T. Mori, Y. Yajima, A wet-chemical process yielding reactive magnesium aluminate spinel (MgAl2O4) powder, Ceram. Int. 27 (2001) 481–489. doi:10.1016/S0272-8842(00)00107-3.

[55] A.P. De Kroon, W. Schafer, F. Aldinger, Crystallography of potassium aluminate K2O.Al2O3, 314 (2001) 147–153.

[56] G. Sciences, Carbonation, hydration, and melting relations in the system MgO-H2O-CO, at pressures up to 100 kbar, Am. Mineral. 64 (1979) 32–40.

[57] L. Xu, H. Song, L. Chou, Ordered mesoporous MgO–Al2O3 composite oxides supported Ni based catalysts for CO2 reforming of CH4: Effects of basic modifier and mesopore structure, Int. J. Hydrogen Energy. 38 (2013) 7307–7325. doi:10.1016/j.ijhydene.2013.04.034.

[58] A. Zhenissova, F. Micheli, L. Rossi, S. Stendardo, P.U. Foscolo, K. Gallucci, Experimental evaluation of Mg- and Ca-based synthetic sorbents for CO2 capture, Chem. Eng. Res. Des. 92 (2014) 727–740. doi:10.1016/j.cherd.2013.11.005.

[59] R. Hadden, J. Howe, K. Waugh, Hydrocarbon steam reforming catalysts- alkali induced resistance to carbon formation, Catal. Deactiv. (1991) 177–184.

[60] B. Acharya, A. Dutta, P. Basu, An investigation into steam gasification of biomass for hydrogen enriched gas production in presence of CaO, Int. J. Hydrogen Energy. 35 (2010) 1582–1589. doi:10.1016/j.ijhydene.2009.11.109.

[61] L. Xu, H. Song, L. Chou, One-Pot Synthesis of Ordered Mesoporous NiO − CaO − Al 2 O 3 Composite Oxides for Catalyzing CO 2 Reforming of CH 4, (2012).

[62] A. Golebiowski, K. Stolecki, U. Prokop, A.Kusmierowska, A. Denis, C. Sikorska, Influence of potassium on the properties of steam reforming catalysts, React.Kinet.Catal.Lett. 82 (2004) 179–189.

[63] H.M. Swaan, V.C.H. Kroll, G.A. Martin, C. Mirodatos, Deactivation of Supported Nickel Catalysts during the Reforming of Methane by Carbon Dioxide, Catal. Today. 21 (1994) 571–578. doi:10.1016/0920-5861(94)80181-9.

[64] K. Engelen, D.J. Draelants, G. V Baron, Improvement of sulphur resistance of a nickel-modified catalytic filter for tar removal from biomass gasification gas, in: Proc. 5th Int. Symp. Gas Clean. High Temp., 2003.

[65] T. Osaki, T. Mori, Role of Potassium in Carbon-Free CO2 Reforming of Methane on K-Promoted Ni/Al2O3 Catalysts, J. Catal. 204 (2001) 89–97. doi:10.1006/jcat.2001.3382.

[66] H.-S. Roh, H.S. Potdar, K.-W. Jun, Carbon dioxide reforming of methane over co-precipitated Ni–CeO2, Ni–ZrO2 and Ni–Ce–ZrO2 catalysts, Catal. Today. 93–95 (2004) 39–44. doi:10.1016/j.cattod.2004.05.012.

[67] J.-S. Chang, D.-Y. Hong, X. Li, S.-E. Park, Thermogravimetric analyses and catalytic

behaviors of zirconia-supported nickel catalysts for carbon dioxide reforming of methane, Catal. Today. 115 (2006) 186–190. doi:10.1016/j.cattod.2006.02.052.

[68] H.J. Park, S.H. Park, J.M. Sohn, J. Park, J.-K. Jeon, S.-S. Kim, et al., Steam reforming of biomass gasification tar using benzene as a model compound over various Ni supported metal oxide catalysts., Bioresour. Technol. 101 Suppl (2010) S101–S103. doi:10.1016/j.biortech.2009.03.036.

[69] W. Chen, G. Zhao, Q. Xue, L. Chen, Y. Lu, High carbon-resistance Ni/CeAlO3-Al2O3 catalyst for CH4/CO2 reforming, Appl. Catal. B Environ. 136–137 (2013) 260–268. doi:10.1016/j.apcatb.2013.01.044.

[70] C.P.B. Quitete, R.C.P. Bittencourt, M.M.V.M. Souza, Steam reforming of tar using toluene as a model compound with nickel catalysts supported on hexaaluminates, Appl. Catal. A Gen. 478 (2014) 234–240. doi:10.1016/j.apcata.2014.04.019.

[71] K. Tomishige, T. Kimura, J. Nishikawa, T. Miyazawa, K. Kunimori, Promoting effect of the interaction between Ni and CeO2 on steam gasification of biomass, Catal. Commun. 8 (2007) 1074–1079. doi:10.1016/j.catcom.2006.05.051.

[72] X. Hu, G. Lu, Inhibition of methane formation in steam reforming reactions through modification of Ni catalyst and the reactants, Green Chem. 11 (2009) 724–732. doi:10.1039/b814009j.

[73] Z. Hou, X.Zheng, T.Yashima, High coke-resistance of K-Ca promoted a-Al2O3 catalyst for CH4 reforming with CO2, React.Kinet.Catal.Lett. 84 (2005) 229–235.

[74] Y.-S. Jung, W.-L. Yoon, Y.-S. Seo, Y.-W. Rhee, The effect of precipitants on Ni-Al2O3 catalysts prepared by a co-precipitation method for internal reforming in molten carbonate fuel cells, Catal. Commun. 26 (2012) 103–111.

doi:10.1016/j.catcom.2012.04.029.

[75] M. Matsumura, C. Hirai, Deterioration Mechanism of Direct Internal Reforming Catalyst, J. Chem. Enginnering Japan. 31 (1998) 734–740.

[76] L. Zhang, B. Zhang, Z. Yang, M. Guo, The Role of Water on the Performance of Calcium Oxide-Based Sorbents for Carbon Dioxide Capture: A Review, Energy Technol. 3 (2015) 10–19. doi:10.1002/ente.201402099.

[77] J. Juan-Juan, M.C. Román-Martínez, M.J. Illán-Gómez, Catalytic activity and characterization of Ni/Al2O3 and NiK/Al2O3 catalysts for CO2 methane reforming, Appl. Catal. A Gen. 264 (2004) 169–174. doi:10.1016/j.apcata.2003.12.040.

[78] M. Demicheli, D. Duprez, J. Barbier, O. Ferretti, E. Ponzi, Deactivation of steam reforming model catalysts by coke formation, J. Catal. 145 (1994) 437–439.

Table 1: Theoretical, actual compositions, and textural properties of 10 wt. % Ni/γ-Al_2O_3 catalysts doped with oxide.

Sample	Theoretical composition (wt. %) ±0.1	Actual composition (wt. %) ±0.1	S_{BET} (m^2/g) ±5	V_p (cm^3/g) ±0.1	V_{DR} (cm^3/g) ±0.01
10Ni	90.0 Al_2O_3 / 10.0 Ni	89.5 Al_2O_3 / 10.5 Ni	240	0.3	0.08
10Ni-1.5Ca	88.5 Al_2O_3 / 10.0 Ni / 1.5 Ca	87.5 Al_2O_3 / 11.1 Ni / 1.5 Ca	240	0.3	0.08
10Ni-1.5K	88.5 Al_2O_3 / 10.0 Ni / 1.5 K	88.0 Al_2O_3 / 10.4 Ni / 1.6 K	235	0.3	0.08
10Ni-1.5Mg	88.5 Al_2O_3 / 10.0 Ni / 1.5 Mg	87.9 Al_2O_3 / 10.8 Ni / 1.3 Mg	230	0.3	0.08
10Ni-1.5Ce	88.5 Al_2O_3 / 10.0 Ni / 1.5 Ce	87.7 Al_2O_3 / 10.6 Ni / 1.7 Ce	245	0.3	0.08
10Ni-1.5Ca-1.5K	87.0 Al_2O_3 / 10.0 Ni /1.5 Ca / 1.5 K	85.8 Al_2O_3 / 11.0 Ni / 1.5 Ca / 1.7 K	255	0.3	0.08
10Ni-1.5Ce-1.5K	87.0 Al_2O_3 /10.0 Ni / 1.5 Ce / 1.5 K	85.5 Al_2O_3 / 11.1 Ni / 1.7 Ce / 1.7 K	245	0.3	0.08
10Ni-3Ca	87.0 Al_2O_3 / 10.0 Ni / 3.0 Ca	86.8 Al_2O_3 / 10.0 Ni / 3.2 Ca	240	0.3	0.08
10Ni-3K	87.0 Al_2O_3 / 10.0 Ni / 3.0 K	85.7 Al_2O_3 / 10.9 Ni / 3.4 K	240	0.3	0.08

S_{BET}: specific surface area determined from nitrogen adsorption-desorption isotherms and using the Brunauer-Emmet-Teller theory; V_p: porous volume determined from nitrogen adsorption-desorption isotherms at saturation pressure; V_{DR}: microporous volume determined from Dubinin-Raduskevitch theory.

Table 2: Ni particle sizes after TPR measurements and total acidity for 10 wt. % Ni/γ-Al_2O_3 catalysts doped with oxide.

Sample	d_{TEM} (nm)	σ_{TEM} (nm)	d_{XRD} (nm) ±1	Weak acid sites ($mmol_{NH3}$/g) ±0.01	Strong acid sites ($mmol_{NH3}$/g) ±0.01	Total acidity ($mmol_{NH3}$/g) ±0.01
10Ni	30	9	23	0.27	0.20	0.47
10Ni-1.5Ca	36	10	26	0.27	0.23	0.50
10Ni-1.5K	38	11	27	0.31	0.19	0.50
10Ni-1.5Mg	34	11	25	0.23	0.24	0.47
10Ni-1.5Ce	44	12	28	-	-	-
10Ni-1.5Ca-1.5K	33	11	27	-	-	-
10Ni-1.5Ce-1.5K	33	10	25	-	-	-
10Ni-3Ca	35	11	26	-	-	-
10Ni-3K	37	10	27	-	-	-

d_{TEM}: metallic particle size median measured with TEM; σ_{TEM} : standard deviation associated to the metallic particle measured with TEM; d_{XRD} : metallic crystallite size estimation obtained by XRD

Table 3: Ni particle sizes after catalytic tests and catalytic performances for 10 wt. % Ni/γ-Al_2O_3 catalysts doped with oxide. Test conditions: T = 650 °C, t = 300 min, 24,000 ppmv of toluene, $GHSV$ = 5000 h^{-1}.

Sample	Ni particles sizes				Catalytic performances				
	d_{TEM} (nm)	σ_{TEM} (nm)	d_{XRD} (nm) ±1	C_T (%) ±1	r_T ($mol_{tolu}/(g_{Ni}.h)$) ±0.1.10^{-2}	C_{CH4} (%) ±1	S_B (%) ±1	*Coke* (g_{Carbon}/g_{Cata}) ±0.01	*Fil. carbon*
10Ni	11	3	12	51	6.7 .10^{-2}	10	15	0.10	No
10Ni-1.5Ca	11	5	10	42	4.9 .10^{-2}	9	6	0.07	No
10Ni-1.5K	12	4	12	55	7.2 .10^{-2}	9	4	0.08	No
10Ni-1.5Mg	11	7	12	31	3.3 .10^{-2}	8	9	0.06	+
10Ni-1.5Ce	8	2	12	50	6.4 .10^{-2}	11	7	0.11	+
10Ni-1.5Ca-1.5K	10	9	12	61	8.6 .10^{-2}	11	4	0.09	No
10Ni-1.5Ce-1.5K	9	3	11	70	1.1 .10^{-1}	10	4	0.11	No
10Ni-3Ca	15	17	19	33	3.9 .10^{-2}	3	7	0.07	+
10Ni-3K	14	13	17	48	6.1 .10^{-2}	7	6	0.02	No

d_{TEM}: metallic particle size median measured with TEM; σ_{TEM} : standard deviation associated to the metallic particle measured with TEM; d_{XRD}: metallic crystallite size estimation obtained by XRD; C_T: conversion of toluene; r_T: reaction rate of toluene; S_B: selectivity in benzene, C_{CH4}: conversion of methane; *Coke*: carbon deposit amount after 5 h of test measured by TG-DSC.

Author Contributions:

Conceptualization and methodology, V.C., T.L., F.M. and S.D.L.; investigation, analysis and writing, V.C., J.G.M., T.L., F.M. and S.D.L., writing-original draft preparation, J.G.M., R.G.T. and S.D.L.; supervision, funding acquisition and project administration, S.D.L. All the authors corrected the paper before submission and during the revision process.

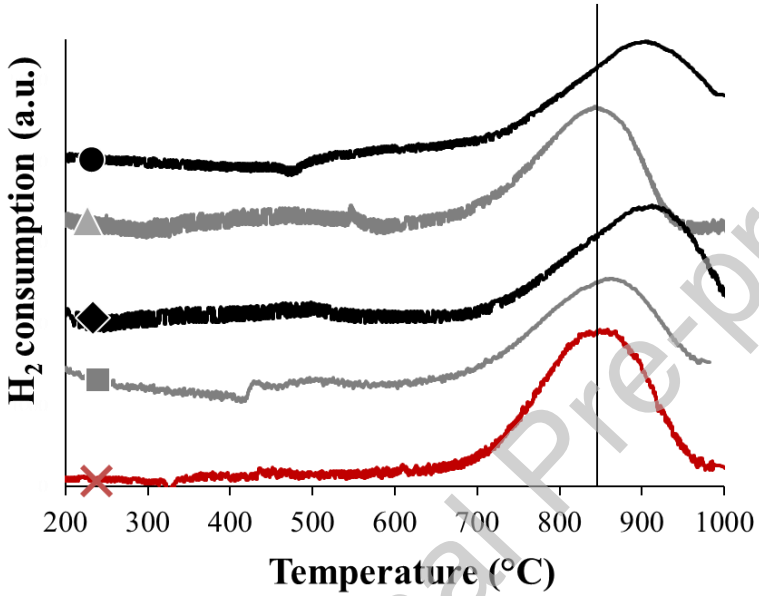

Figure 1: H_2-TPR curves for 10 wt. % Ni/γ-Al_2O_3 catalysts doped with 1.5 wt. % of oxide: (×) 10Ni, (■) 10Ni-1.5Ca, (♦) 10Ni-1.5Mg, (▲) 10Ni-1.5K, and (●) 10Ni-1.5Ce.

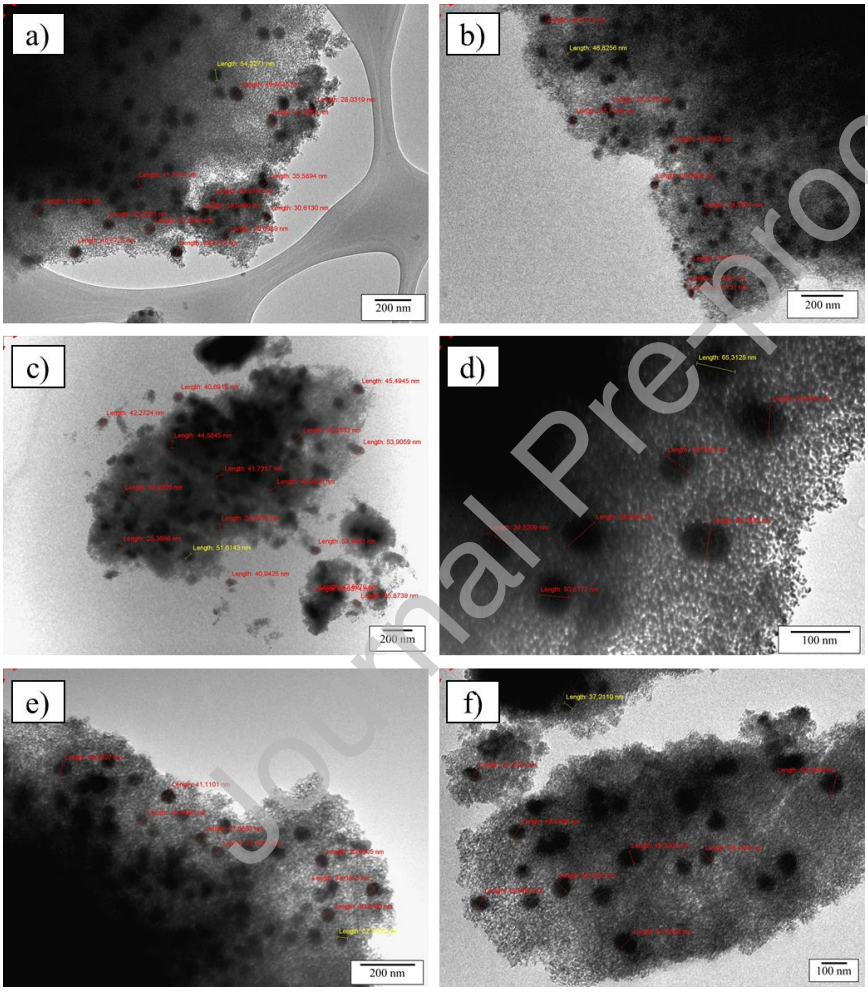

Figure 2: TEM observations after TPR measurements of Ni/γ-Al_2O_3 catalysts: (a) 10Ni-1.5Ca, (b) 10Ni-1.5Mg, (c) 10Ni-1.5K, (d) 10Ni-1.5Ce, (e) 10Ni-1.5Ce-1.5K and (f) 10Ni-3K.

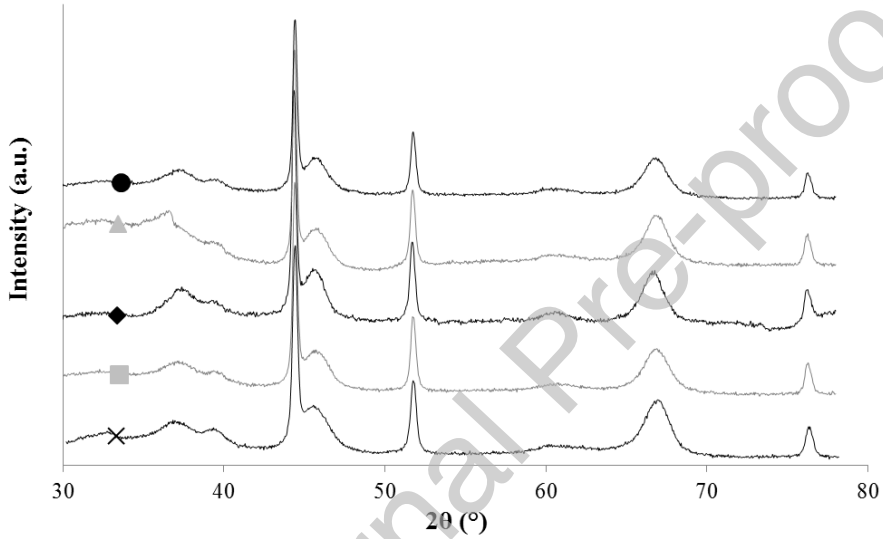

Figure 3: XRD diffractograms after TPR measurements for 10 wt. % Ni/γ-Al_2O_3 catalysts doped with 1.5 wt. % of oxide: (×) 10Ni, (■) 10Ni-1.5Ca, (♦) 10Ni-1.5Mg, (▲) 10Ni-1.5K, and (●) 10Ni-1.5Ce.

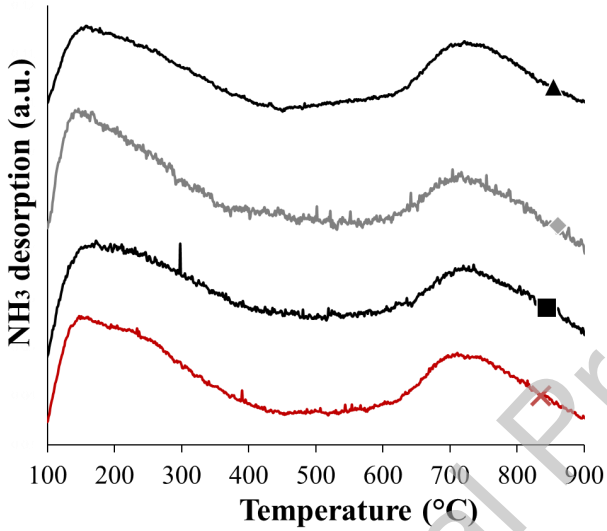

Figure 4: NH_3-TPD curves for 10 wt. % Ni/γ-Al_2O_3 catalysts doped with 1.5 wt. % of alkali: (×) 10Ni, (■) 10Ni-1.5Ca, (♦) 10Ni-1.5Mg, and (▲) 10Ni-1.5K.

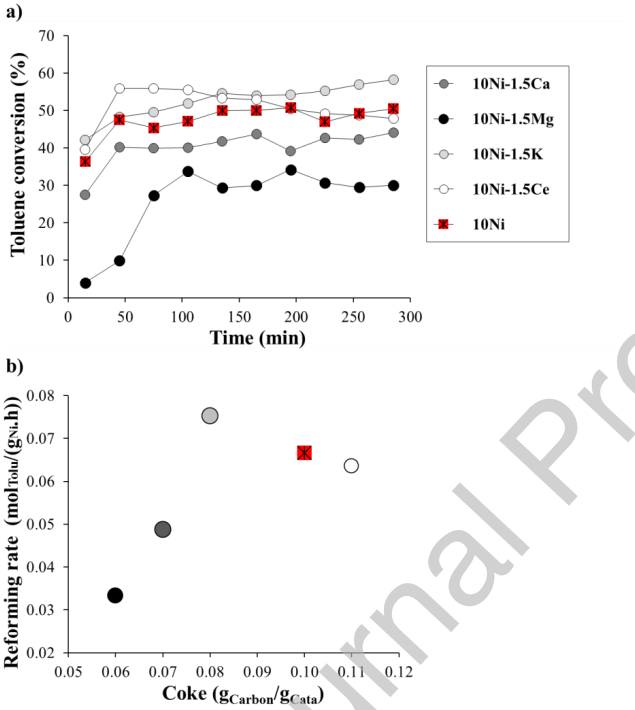

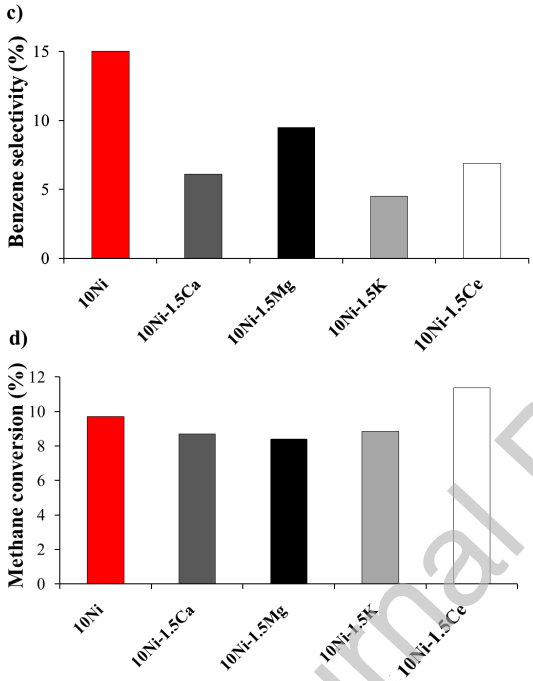

Figure 5: (a) Toluene conversion as a function of time; (b) toluene reforming rate as a function of carbon deposit amount; (c) benzene selectivity and (d) methane conversion diagrams for 10 wt. % Ni/γ-Al_2O_3 catalysts doped with 1.5 wt. % of oxide.

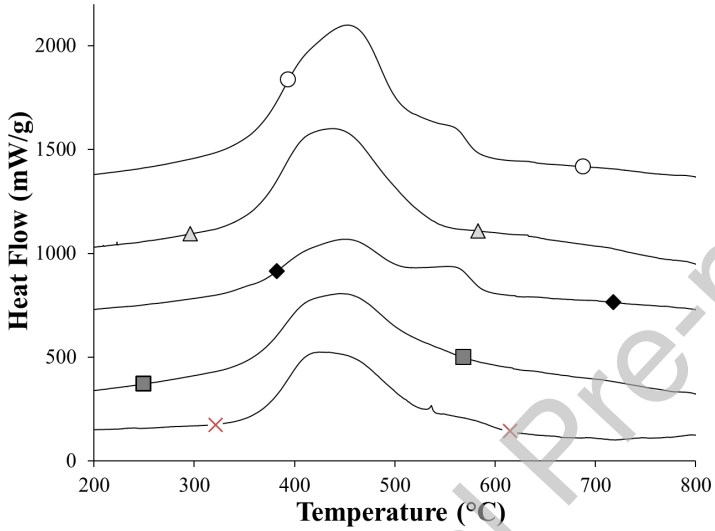

Figure 6: Post-test DSC curves for 10 wt. % Ni/γ-Al_2O_3 catalysts doped with 1.5 wt. % of oxide: (×) 10Ni, (■) 10Ni-1.5Ca, (♦) 10Ni-1.5Mg, (▲) 10Ni-1.5K, and (●) 10Ni-1.5Ce.

a)

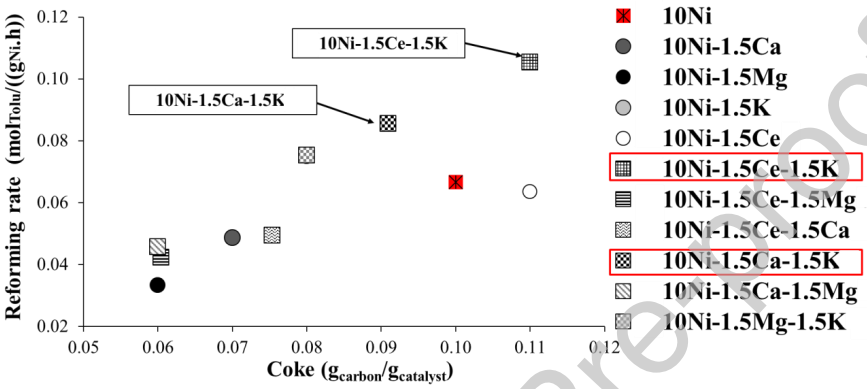

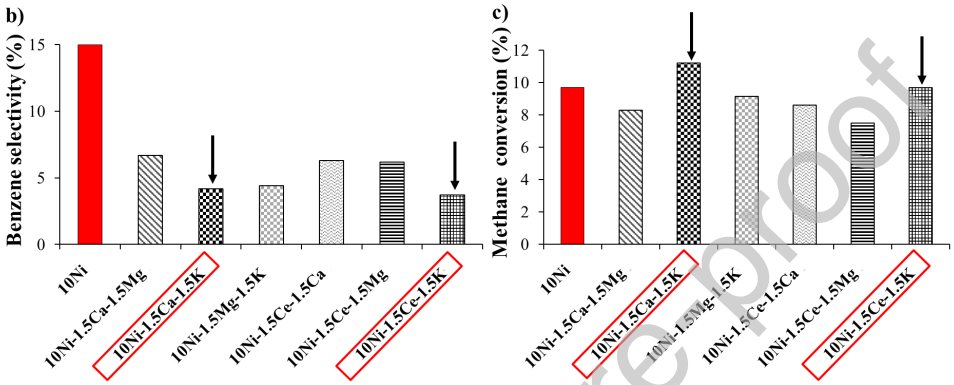

Figure 7: (a) Toluene reforming rate as a function of carbon deposit; (b) benzene selectivity, and (c) methane conversion diagrams for 10 wt. % Ni/γ-Al_2O_3 catalysts doped with 1.5 wt. % of two different oxides.

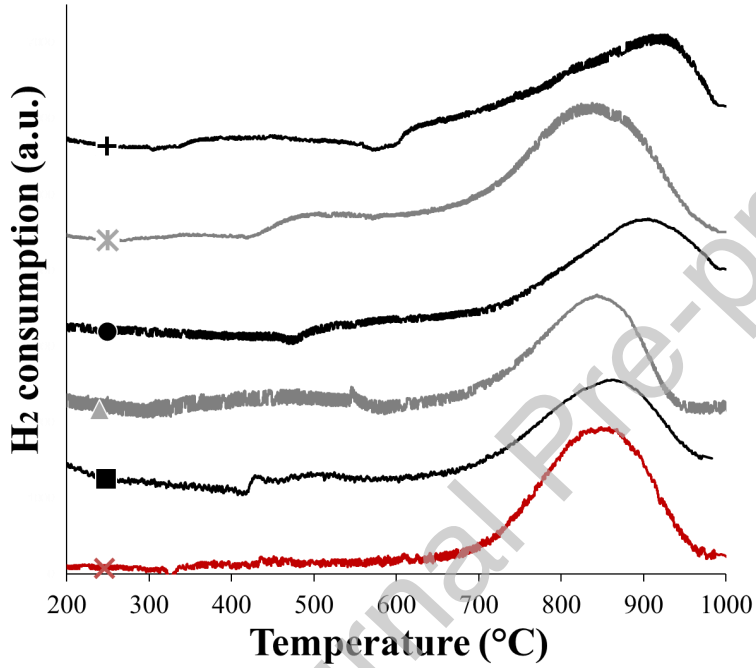

Figure 8: TPR profiles of samples doped with 1.5 wt. % of oxide or with two oxides: (×) 10Ni, (■) 10Ni-1.5Ca, (▲) 10Ni-1.5K, (●) 10Ni-1.5Ce, (∗) 10Ni-1.5Ca-1.5K, and (+) 10Ni-1.5Ce-1.5K.

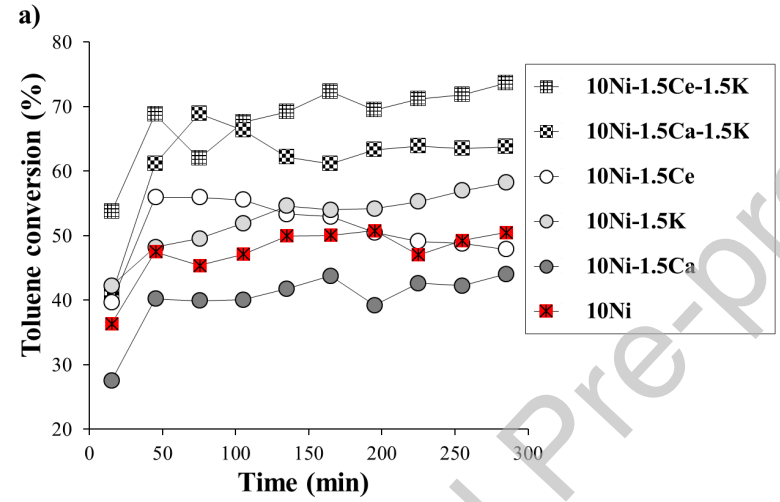

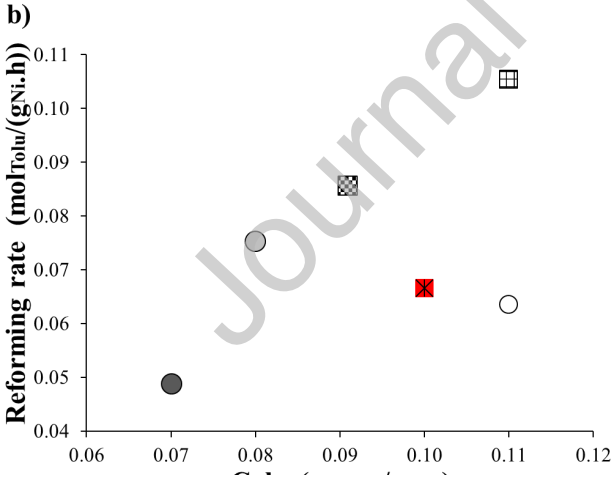

Figure 9: (a) Toluene conversion as a function of time and (b) toluene reforming rate as a function of carbon deposit amount for samples 10Ni-1.5Ca-1.5K, 10Ni-1.5Ce-1.5K, 10Ni-1.5Ca, 10Ni-1.5K, 10Ni-1.5Ce, and 10Ni.

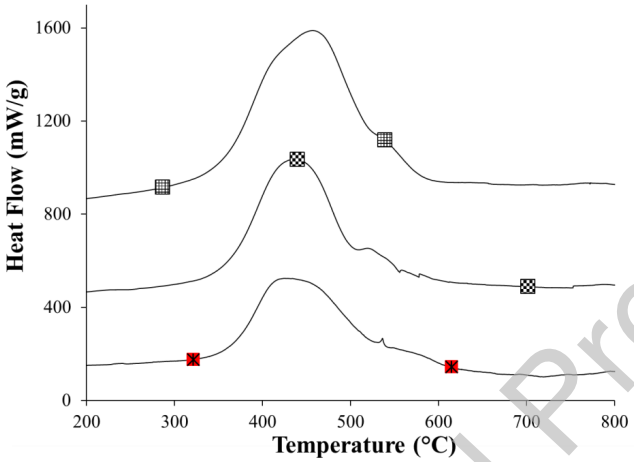

Figure 10: Post-test DSC curves for double oxides doped catalysts; (▩) 10Ni, (▩) 10Ni-1.5Ca-1.5K, and (▩) 10Ni-1.5Ce-1.5K.

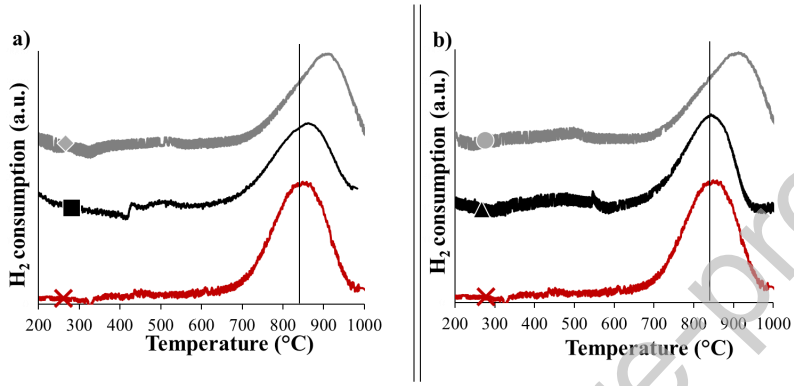

Figure 11: TPR profiles for 10 wt. % Ni/γ-Al_2O_3 catalysts doped with different loadings of (a) Ca: (×) 10Ni; (■) 10Ni-1.5Ca; (♦) 10Ni-3Ca; and (b) K: (×) 10Ni; (▲) 10Ni-1.5K; and (●) 10Ni-3K.

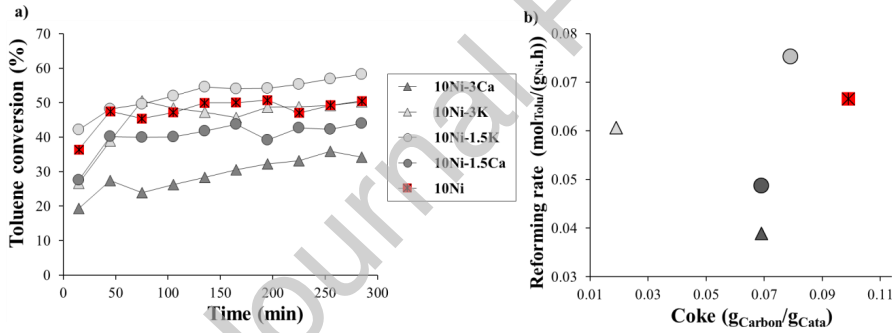

Figure 12: (a) Toluene conversion as a function of time and (b) toluene reforming rate as a function of carbon deposit amount for 10 wt. % Ni/γ-Al_2O_3 catalysts doped with different loadings of Ca or K.

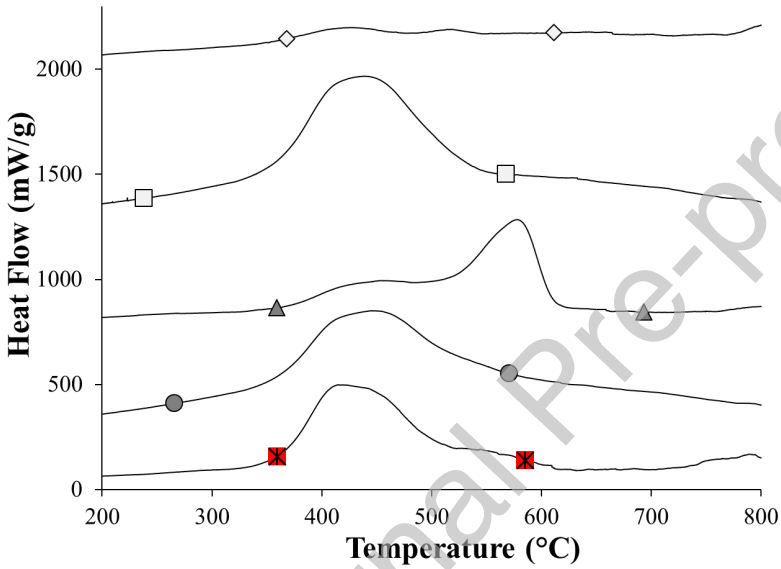

Figure 13: Post-test DSC curves for 10 wt. % Ni/γ-Al_2O_3 catalysts doped with different loadings of Ca or K: (✱) 10Ni, (●) 10Ni-1.5Ca, (▲) 10Ni-3Ca, (■) 10Ni-1.5K, and (♦) 10Ni-3K.

G A